ChemComm
Chemical Communications

Accepted Manuscript

This article can be cited before page numbers have been issued, to do this please use: X. Wang, S. Feng, D. He and P. Jiang, *Chem. Commun.*, 2020, DOI: 10.1039/D0CC06209J.

ROYAL SOCIETY OF CHEMISTRY

rsc.li/chemcomm

Cite this: DOI: 10.1039/c0xx00000x

www.rsc.org/xxxxxx

ARTICLE TYPE

Porous manganese-cobalt oxide microsphere with tunable oxidase mimicking activity for sulfide ion colorimetric detection

Xue Wang, Shiya Feng, Daiping He*, and Ping Jiang*

Received (in XXX, XXX) Xth XXXXXXXXX 20XX, Accepted Xth XXXXXXXXX 20XX
DOI: 10.1039/b000000x

Here, we report the controllable synthesis of porous $Mn_xCo_{1-x}O$ microsphere and the tunable catalytic activity in oxidase mimicking reaction. $Mn_{0.6}Co_{0.4}O$ owns the best oxidase-like mimicking activity and can be used successfully in sulfide ion colorimetric detection with a low detection limit of 0.1 μM.

Since the magnetic iron oxide nanoparticles was reported with intrinsic peroxidase-like activity,[1] a diverse range of nanomaterials including transition metal oxides,[2] precious metals,[3] carbon materials[4] and metal-organic-frameworks (MOF)[5] have been explored as efficient functional catalysts to mimic natural enzyme in biosensing, immunoassays, clinical therapy and environmental protection. Compared with the peroxidase-like activities have been discovered by most of these nanostructures, the oxidase-like activities were found concentrating mainly on Pt-group metals nanomaterials.[3,6-8] Although oxidase-like mimicking reaction was simpler than that of peroxidase-like mimics which need the mediation of H_2O_2, the high cost and low availability of Pt-group metals impede its widespread application. Therefore, it is highly attractive to explore oxidase-like nanoenzymes made from cost-effective and earth-abundant elements.

Since oxidase mimicking reaction and electrochemical oxygen reduction reaction (ORR) share the similar reaction process and catalytic mechanism, which rely on the catalyst to reversibly bind O_2, and O_2 decomposed to produce reactive oxygen species (ROS), the ORR catalysts hold a great promising to be candidates for oxidase mimics.[9,10] Indeed, some noble-metal-free ORR electrocatalysts such as Co,N co-doped porous carbon,[11] Fe_3C@C,[9] and Fe-N-C[12, 13] have been recently identified as efficient oxidase mimics. Manganese oxides, which have gained a substantial amount of attention in ORR due to the abundance, low-cost, and moderate ability of binding O_2,[14,15] have recently been demonstrated as highly efficient oxidase mimics in biosensing.[2,16] Unfortunately, it was found that MnO_2 was unstable in the enzyme mimicking reaction and tend to be reduced by organic dyes, along with complete dissolution in reaction system.[2,17,18]

Given that mixed manganese oxides such as Mn-Co oxide shows remarkable high stability and efficiency in oxygen reduction and evolution reaction,[19,20] it is expected that engineering mixed Mn oxide maybe offers MnO_2 oxidase mimic with outstanding high stability and activity. However, few studies focus on engineering mixed Mn oxide nanoenzyme. Gao *et al.*[21] have recently prepared $MnCo_2O_4$ nanofibers using electrospinning technique and utilized it as oxidase mimic for sulfite and L-cysteine colorimetric detection, but its synthesis suffers from complicate operation and the involvement of several organic solvents. Moreover, the fixed Mn content in $MnCo_2O_4$ lose the ability in tuning the adsorption of O_2 on the catalyst surface to get the optimal catalytic activity. Zhang *et al.*[22] engineered Mn/Co oxides as oxidase in colorimetric sensing of acid phosphatase, however, it has a hybrid composition consisting of Mn_2O_3 and $CoMn_2O_4$.

Herein, a simple and controllable approach was presented to prepare porous $Mn_xCo_{1-x}O$ (*x* represents molar fraction in metal composition) microsphere through annealing Mn-Co Prussian blue analogues (PBA) precursor. By varying Mn/Co molar ratio in the Mn-Co PBA precursor, the tune of Mn content and the exploration of corresponding composition-activity relationship for $Mn_xCo_{1-x}O$ were also successfully realized. The best oxidase-like mimicking activity was achieved when the composition is $Mn_{0.6}Co_{0.4}O$. Due to the strong color fading effect on oxidized blue 3,3′,5,5′-tetramethylbenzidine (oxTMB), sulfide ion can be sensitively detected using this colorimetric approach, with a low detection limit of 0.1 μM.

$Mn_xCo_{1-x}O$ was prepared via a two-step method, with the first step to prepare Mn-Co PBA with different Mn content, and the second step to anneal the resulting Mn-Co PBA precursor under air condition. Fig. 1a shows the X-ray diffraction (XRD) patterns for $Mn_{0.6}$-$Co_{0.4}$ PBA (blue curve) and the annealed product (red curve), respectively. As observed, the $Mn_{0.6}$-$Co_{0.4}$ PBA precursor shows diffraction peaks characteristic of $Mn_3[Co(CN)_6]_2 \cdot 9H_2O$ (JCPDS No. 51-1898), and the resulting product (red curve) only shows peaks assigned to $(Co,Mn)(Co,Mn)_2O_4$ (JCPDS No. 18-0408), indicating the successful synthesis of Mn-Co oxide. Since no additional peaks from impurities are detected, it suggests the high purity of the resulted Mn-Co oxide. Here,

View Article Online
DOI: 10.1039/D0CC06209J

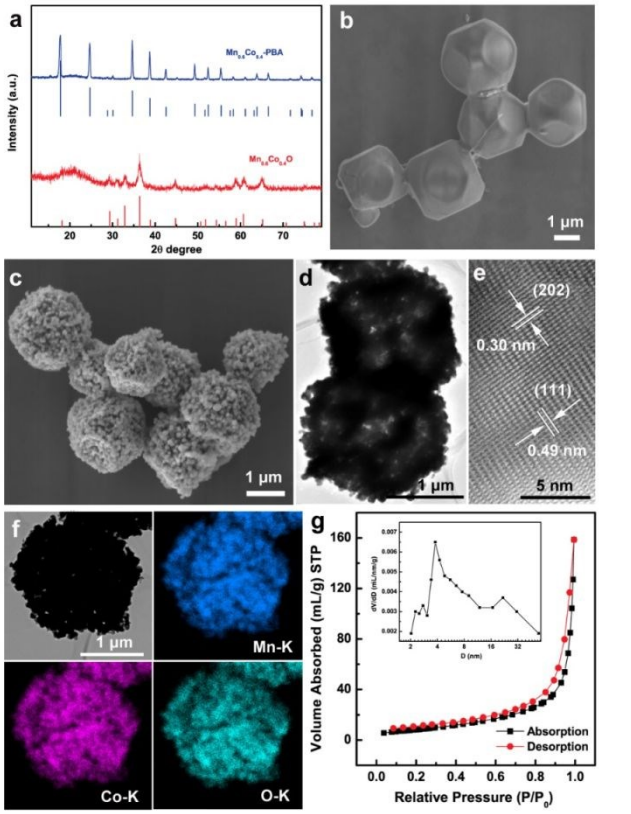

Fig. 1. (a) XRD patterns for $Mn_{0.6}$-$Co_{0.4}$ PBA and $Mn_{0.6}Co_{0.4}O$. (b) and (c) SEM images for $Mn_{0.6}$-$Co_{0.4}$ PBA and $Mn_{0.6}Co_{0.4}O$, respectively. (d) low- and (e) high-magnification TEM images of $Mn_{0.6}Co_{0.4}O$. (f) STEM image and EDX elemental mapping of Mn, Co, and O for $Mn_{0.6}Co_{0.4}O$. (g) Nitrogen adsorption/desorption isotherm plot and BJH pore-size distribution curve (inset) for porous $Mn_{0.6}Co_{0.4}O$ microsphere.

the Mn-Co oxide was denoted as $Mn_{0.6}Co_{0.4}O$ (0.6 and 0.4 represent Mn and Co molar fraction, respectively). Figure 1b displays the scanning electron microscopy (SEM) images of $Mn_{0.6}$-$Co_{0.4}$ PBA, indicating they are dice-like morphology with diameters about 2-3 μm and smooth surface. Annealing these precursors gives porous $Mn_{0.6}Co_{0.4}O$ microsphere with decreased diameter ranging from 1.5 to 2 μm (Fig. 1c). These porous microspheres are clearly made of interconnected nanoparticles of $Mn_{0.6}Co_{0.4}O$ (Fig. 1c and d). Fig. 1e presents HRTEM image taken from one single nanocrystal, revealing clear lattice fringes with interplane distance of 0.30 and 0.49 nm, which can be well ascribed to the (202) and (111) plane of $Mn_{0.6}Co_{0.4}O$, respectively. Fig. 1f shows the scanning TEM (STEM) image and the corresponding EDX elemental mapping images (Fig. 1f) of Mn, Co and O for $Mn_{0.6}Co_{0.4}O$ microsphere, clearly revealing its porous structure and the uniformly distribution of these elements over the entire microsphere. Furthermore, Fig. S1 shows EDX spectrum of $Mn_{0.6}Co_{0.4}O$, indicating a 1.42:1 Mn:Co atomic ratio, consistent within experimental error with the expected 1.5:1 stoichiometry of $Mn_{0.6}Co_{0.4}O$. The Brunauer-Emmett-Teller (BET) specific surface area (SSA) of $Mn_{0.6}Co_{0.4}O$ microsphere was determined to be 31.4 $m^2\ g^{-1}$ by the nitrogen adsorption/desorption isotherm plot, and the Barrett-Joyner-Halenda (BJH) pore-size distribution curve shows a sharp peak at 3.9 nm, which was resulted from the interconnection of $Mn_{0.6}Co_{0.4}O$ nanocrystallites inside the microsphere (Fig. 1g). All these results demonstrate the successful synthesis of porous Mn-Co oxide via annealing Mn-Co PBA precursor.

To further probe the chemical composition and elemental valence state of the $Mn_{0.6}Co_{0.4}O$, X-ray photoelectron spectroscopy (XPS) analysis was conducted (Fig. S2a). The survey spectrum evidences the presence of Mn, Co, O and C from the reference. The high-resolution Mn 2p spectrum (Fig. S2b) shows two peaks at 641.8 and 653.3 eV with a separation of 11.5 eV, corresponding to Mn $2p_{3/2}$ and Mn $2p_{1/2}$, respectively. The deconvoluted peaks at 641.7 and 653.2 eV can be ascribed to the existence of Mn^{2+} and the other two peaks at 643.8 and 654.0 eV can be attributed to Mn^{3+}.[19,20] Co 2p XPS spectrum (Fig. S2c) also shows two main peaks at 780.2 and 795.4 eV assigned to Co $2p_{3/2}$ and Co $2p_{1/2}$, respectively. Besides, two shake-up satellites peaks are observed at 786.7 and 803.2 eV. The fitted peaks at 781.7 and 797.4 eV are indexed to Co^{2+}, while the other two peaks at 780.1 and 795.3 eV are ascribed to the Co^{3+}.[19,20] Fig. S2d show the high-resolution O 1s spectrum, the deconvoluted peaks at 529.8 and 531.7 eV indicates O species in the metal-oxygen bonding and in surface defect sites, respectively.[22,23] The above results reveal the as-prepared $Mn_{0.6}Co_{0.4}O$ possess multiple solid-state redox couples (Mn^{2+}/Mn^{3+}, Co^{2+}/Co^{3+}), implying a great potential in enzyme mimic catalysis reaction.

The oxidase-like activity of $Mn_{0.6}Co_{0.4}O$ was investigated by using the well-established probe reaction, the oxidation of 3,3′,5,5′-tetramethylbenzidine (TMB) without the addition of H_2O_2. As shown in Fig. 2a, the solution containing either 50 μM TMB or 8 μg/mL $Mn_{0.6}Co_{0.4}O$ appears colorless, while it rapidly turns to dark blue once they are mixed. The characteristic blue color and absorbance at 652 nm strongly confirms the appearance of oxTMB, suggesting the catalytic activity of $Mn_{0.6}Co_{0.4}O$ in TMB oxidation. It is important to note that annealing Mn-Co PBA precursor with different Mn content gives pure Mn-Co oxide composed of single $Mn_xCo_{1-x}O$ phase (Fig. 2b) and shows the similar catalytic activity in TMB oxidation. To gain more insight, Co_3O_4 and MnO_2 (Fig. S3) were also studied for comparison. As shown in Fig. 2c, Co_3O_4 shows poor catalytic activity for TMB oxidation. In sharp contrast, MnO_2 displays remarkable high performance in TMB oxidation reaction. Furthermore, with the doping of Co, the catalytic activity of $Mn_xCo_{1-x}O$ nanoenzyme climbs and reaches to peak level when x value achieved 0.6 (Fig. 2c and d). These findings demonstrate the crucial role of Co element in tuning Mn-Co oxide performance in catalyzing TMB oxidation. The definite composition-activity relationship for $Mn_xCo_{1-x}O$ oxidase mimic, to the best of our knowledge, was firstly established.

View Article Online
DOI: 10.1039/D0CC06209J

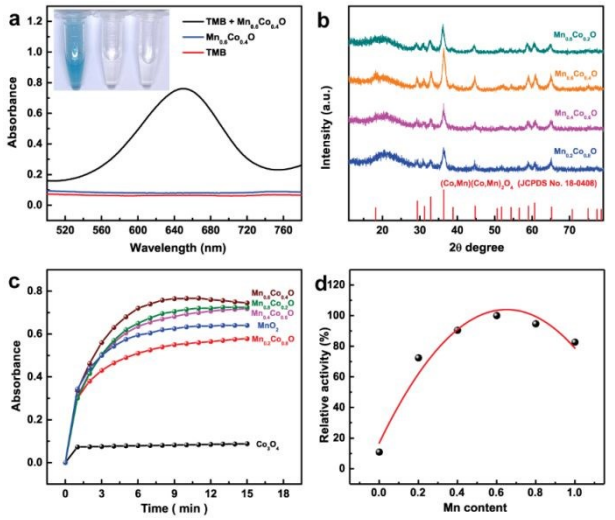

Fig. 2. (a) The absorption spectra of TMB, $Mn_{0.6}Co_{0.4}O$, and their mixture. Inset shows the corresponding photograph. (b) XRD patterns of $Mn_xCo_{1-x}O$. (c) Time-dependent absorbance change of oxTMB at 652 nm for $Mn_xCo_{1-x}O$ and (d) the corresponding composition-activity relationship. Reaction conditions: 50 μM TMB, 8 μg/mL $Mn_xCo_{1-x}O$, 0.2 M HAc-NaAc buffer (pH 5), 20 °C.

It should be noted that pyrolysis temperature has an important effect on Mn-Co oxide composition, as well as the oxidase mimicking activity. As shown in Fig. S4a, the pyrolysis product at lower temperature (300 to 500 °C) contains pure $(Co,Mn)(Co,Mn)_2O_4$ phase, while it becomes hybrid composition when temperature reaches to 600 °C, due to the appearance of $MnCo_2O_4$. The oxidase-like activities of these pyrolysis products were evaluated (Fig. S4b). Obviously, Mn-Co oxide obtained at 400 °C displays the higher catalytic activity than others. Because catalytic reaction always occurs at the surface of catalyst, the larger specific surface area (SSA) is considered beneficial for oxidase-like activity. Here, the SSA of Mn-Co oxide achieved at 300, 400, 500 and 600 °C were determined to be 24.9, 31.4, 29.6 and 20.4 m^2/g, respectively. Therefore, it is safely to infer that the higher catalytic activity of $Mn_{0.6}Co_{0.4}O$ obtained at 400 °C was mainly ascribed to its larger SSA. Therefore, the $Mn_{0.6}Co_{0.4}O$ obtained at 400 °C was selected and utilized as oxidase mimic for our further exploration.

The mechanism for $Mn_{0.6}Co_{0.4}O$ in catalyzing TMB oxidation was further investigated. In general, generation of active oxygen species (ROS) and accelerating electron transfer process are two most possible mechanisms responsible for oxidase mimicking activity.[10,24] Here, we firstly conducted N_2 purge experiment to estimate the role of the dissolve oxygen in enzyme mimicking reaction. As observed in Fig. S5a, the absorption at 652 nm decreased when it has undergone N_2 purging for 30 min before the addition of TMB, demonstrating the participation of the dissolved oxygen in this color reaction. According to previous reports,[25] dissolved oxygen can be activated on nanoenzyme surface to generate ROS such as •OH and $O_2^{\bullet-}$, which are responsible for TMB oxidation reaction. These ROS can be verified using radical scavenging experiments (Fig. S5b). As shown, the addition of ascorbic acid (AA) (•OH and $O_2^{\bullet-}$ scavengers), thiourea (·OH scavengers), and p-benzoquinone (p-BQ) ($O_2^{\bullet-}$ scavengers) with different level simultaneously cause decrease in absorption at 652 nm, implying the produce of •OH and $O_2^{\bullet-}$ during the catalytic process.[22] These findings demonstrated that the oxidase-like activity of $Mn_{0.6}Co_{0.4}O$ was mainly attributed to its ability in catalyzing dissolved oxygen to generate ROS.

Similar to other nanoenzymes, the oxidase mimicking activity of $Mn_{0.6}Co_{0.4}O$ was dependent on reaction solution pH, catalyst concentration and reaction temperature. Fig. S6a-c shows the absorbance changes at 652 nm of the reaction system under different pH, $Mn_{0.6}Co_{0.4}O$ concentration and reaction temperature. Obviously, the maximum catalytic activity was achieved when the pH was set to 5, the catalyst concentration was 8 μg/mL, and the incubation temperature was 20 °C.

Under the optimum conditions, we further explore the catalytic efficiency of $Mn_{0.6}Co_{0.4}O$ via steady-state kinetic experiments (Fig. S7). The K_m and V_{max} were calculated to be 0.0187 mM and 7.62×10^{-8} M/s, respectively. The K_m value of $Mn_{0.6}Co_{0.4}O$ was two times lower than that of Mn/Co oxides nanocomposites (0.0378 mM)[22] and $CNF/MnCo_2O_{4.5}$ (0.04 mM),[21] suggesting higher affinity and more accessibility to TMB substrate for present $Mn_{0.6}Co_{0.4}O$. Such superior catalytic activity, might be attributed to its porous structure with large SSA, as well as the rich solid-state redox couples on $Mn_{0.6}Co_{0.4}O$ surface.

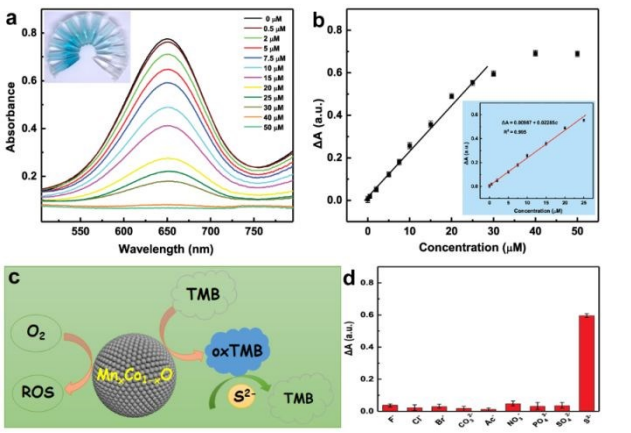

Fig. 3. (a) Typical absorption spectra of TMB-$Mn_{0.6}Co_{0.4}O$ system in the presence of different sulfide ions. Reaction conditions: 8 μg/mL $Mn_{0.6}Co_{0.4}O$, 50 μM TMB, 0.2 M HAc-NaAc buffer (pH 5.0). Inset shows the corresponding photograph. (b) The corresponding plot of absorbance vs the concentration of S^{2-} in the range of 0-50 μM. Inset shows the linear correlation part. (c) Schematic of oxidase-like activity of $Mn_xCo_{1-x}O$ and its application for S^{2-} sensing. (d) The decreased absorbance at 652 nm caused by the addition of 30 μM S^{2-} and 300 μM other interferents. Reaction conditions: 8 μg/mL $Mn_{0.6}Co_{0.4}O$, 50 μM TMB, 0.2 M HAc-NaAc buffer (pH 5), 20 °C.

DOI: 10.1039/D0CC06209J

As a traditional toxic pollutant, S^{2-} detection has caused a great concern in biological and environmental fields. Due to the simple operation and rapid detection, S^{2-} colorimetric detection has attracted great interests and tremendous efforts in recent years.[26,27] Intriguingly, it is found that sulfide ion has a color fading effect on oxidized blue TMB substrate with a linear relationship between its concentration and the declined absorbance (Fig. 3a and b). Therefore, a simple and novel oxidase based colorimetric method for S^{2-} detection can be presented. The fading effect should be ascribed to the reaction between oxidized blue TMB (oxTMB) and reductive sulfide ion (Fig. 3c), just like that between oxTMB and glutathione.[2] As shown in Fig. 3b inset, the present colorimetric detection of S^{2-} exhibits a wider linear range from 0 to 25 μM, and a low detection limit of 0.1 μM (S/N = 3). Such performances were superior than other S^{2-} colorimetric sensors such as Ag NPs,[27] Cu NCs,[26] and Au NPs[28] (Tab. S2).

To evaluate the feasibility of the present colorimetric sensor, the selectivity for S^{2-} detection was also investigated. Fig. 3d shows the decreased absorption at 652 nm caused by the introduce of 30 μM S^{2-} and 300 μM other common interferents. The decreased absorption caused by interferents was obviously negligible in comparison with that caused by S^{2-}, suggesting excellent selectivity of this method. The reliability of this sensor was further assessed by monitoring S^{2-} concentration in tap water. According to previous reports,[26,28] there are too low S^{2-} to be detected in tap water, therefore, the recovery experiment was conducted to demonstrate its reliability. As shown in Tab. S3, the recovery for the sample was in the range of 100.8-103.3% with the relative standard deviation (RSD) less than 5%, suggesting the good promising in using the present S^{2-} sensor in environment monitoring.

In summary, porous $Mn_xCo_{1-x}O$ microsphere was prepared and used as noble-metal free oxidase mimic for sulfide ion colorimetric detection. $Mn_xCo_{1-x}O$ with pure phase and tunable composition was successfully realized through annealing Mn-Co PBA precursor. The composition-activity relationship for $Mn_xCo_{1-x}O$ oxidase mimic was firstly established, and $Mn_{0.6}Co_{0.4}O$ was demonstrated as the best oxidase-mimics. The superior activity should be contributed to the larger SSA originated from the porous structure, as well as the multiple redox couples in $Mn_xCo_{1-x}O$ surface. Due to the color fading effect of sulfide ion on oxidized blue TMB, a sensitive colorimetric sulfide ion detection method was developed. This work not only paves a new way for accurate control synthesis binary metal oxide with high catalytic activity in oxidase mimicking reaction, but explores a new noble-metal free oxidase mimic for sulfide ion detection in environment monitoring.

This work was supported by the National Natural Science Foundation of China (Grant No. 21601022), the NSF of Chongqing (Grant No. cstc2018jcyjAX0698 and cstc2019jcyj-msxmX0528), and Program for Leading Talents of Scientific Innovation of Chongqing Normal University.

Conflicts of interest

There are no conflicts to declare.

Notes and references

Chongqing Key Laboratory of Green Synthesis and Applications, College of Chemistry, Chongqing Normal University, Chongqing 401331, China. E-mail: hedaiping@126.com; jphdp868@126.com.

† Electronic Supplementary Information (ESI) available: Exprimental details, SEM and TEM iamges, absorbance curve, kinetic assays. See DOI: 10.1039/x0xx00000x

1 L. Gao, J. Zhuang, L. Nie, J. Zhang, Y. Zhang, N. Gu, T. Wang, J. Feng, D. Yang, S. Perrett and X. Yan, *Nat. Nanotech.,* 2007, **2**, 577-583.
2 J. Liu, L. Meng, Z. Fei, P. J. Dyson, X. Jing and X. Liu, *Biosens. Bioelectron.,* 2017, **90**, 69-74.
3 M. Huang, H. Wang, D. He, P. Jiang and Y. Zhang, *Chem. Commun.,* 2019, **55**, 3634-3637.
4 Y. Hu, X. J. Gao, Y. Zhu, F. Muhammad, S. Tan, W. Cao, S. Lin, Z. Jin, X. Gao and H. Wei, *Chem. Mater.* 2018, **30**, 6431-6439.
5 J. Chen, Q. Wang, L. Huang, H. Zhang, K. Rong, H. Zhang and S. Dong, *Nano Res.,* 2018, **11**, 4905-4913.
6 Y. Zhan, Y. Zeng, L. Li, L. Guo, F. Luo, B. Qiu, Y. Huang and Z. Lin, *Anal. Chem.,* 2020, **92**, 1236-1244.
7 J. Liu, X. Hu, S. Hou, T. Wen, W. Liu, X. Zhu, J.-J. Yin and X. Wu, *Sensor. Actuat B-Chem.,* 2012, **166**, 708-714.
8 H. Z. Fan, Y. Y. Li, J. B. Liu, R. Cai, X. S. Gao, H. Zhang, Y. L. Ji, G. J. Nie and X. C. Wu, *ACS Appl. Mater. Interf.,* 2019, **11**, 45416-45426.
9 H. Yang, J. Xiao, L. Su, T. Feng, Q. Lv and X. Zhang, *Chem. Commun.,* 2017, **53**, 3882-3885.
10 H. Yang, J. Xiao, J. Shi, T. Shu, L. Su, Q. Lu and X. Zhang, *Chem. Commun.,* 2018, **54**, 818-820.
11 S. Li, L. Wang, X. Zhang, H. Chai and Y. Huang, *Sensor. Actuat B-Chem.,* 2018, **264**, 312-319.
12 F. He, L. Mi, Y. Shen, T. Mori, S. Liu and Y. Zhang, *ACS Appl. Mater. Interf.,* 2018, **10**, 35327-35333.
13 Q. Chen, S. Li, Y. Liu, X. Zhang, Y. Tang, H. Chai, Y. Huang, *Sensor. Actuat B- Chem.,* 2020, **305**, 127511.
14 F. Cheng, T. Zhang, Y. Zhang, J. Du, X. Han and J. Chen, *Angewa. Chem. Int. Ed.,* 2013, **52**, 2474-2477.
15 O. Keisar, Y. Ein-Eli, Y. Alfi and Y. Cohen, *J. Power. Source.,* 2020, **450**, 227545.
16 X. Zhang, X. Mao, S. Li, W. Dong and Y. Huang, *Sensor. Actuat B-Chem.,* 2018, **258**, 80-87.
17 J. Zhang, X. Dai, Z.- L. Song, R. Han, L. Ma, G. C. Fan and X. Luo, *Sensor. Actuat B- Chem.,* 2020, **304**, 127304.
18 P. Chen, H. Zhong, X. Wang, C. Shao, S. Zhi, X. R. Li and C. Wei, *Anal. Method.*, 2019, **11**, 1469-1474.
19 H. Yang, M. Zhu, X. Guo, C. Yan and S. Lin, *ACS Omega.*, 2019, **4**, 22325-22331.
20 J. Li, Y. Zhang, L. Li, Y. Wang, L. Zhang, B. Zhang, F. Wang, B. Li and X. Y. Yu, *Dalton. T.,* 2019, **48**, 17022-17028.
21 M. Gao, X. Lu, M. Chi, S. Chen and C. Wang, *Inorg. Chem. Front.,* 2017, **4**, 1862-1869.
22 X. Zhang, A. Yuan, X. Mao, Q. Chen and Y. Huang, *Sensor. Actuat B-Chem.,* 2019, **299**, 126928.
23 N. T. Dung, T. V. Thu, T. Van Nguyen, B. M. Thuy, M. Hatsukano, K. Higashimine, S. Maenosono and Z. Zhong, *RSC Adv.,* 2020, **10**, 3775-3788.
24 G. J. Cao, X. Jiang, H. Zhang, T. R. Croley and J. J. Yin, *RSC Adv.,* 2017, **7**, 52210-52217.
25 H. Wei and E. Wang, *Chem. Soc. Rev.,* 2013, **42**, 6060-6093.
26 H. Liao, L. Hu, Y. Zhang, X. Yu, Y. Liu and R. Li, *Microchim. Acta.,* 2018, **185**, 143.
27 K. Shanmugaraj and M. Ilanchelian, *Microchim. Acta.,* 2016, **183**, 1721-1728.
28 H. Deng, G. Wu, X. Lin, X. Xu, A. Liu, X. Xia and W. Chen, *RSC Adv.,* 2015, **5**, 58574-58579.

Porous $Mn_xCo_{1-x}O$ microsphere derived from Mn-Co PBA with tunable oxidase-like activity and high efficiency in S^{2-} colorimetric detection